Author(s): Tuovinen, Toni & Hinkkanen, Marko

Title: Adaptive Full-Order Observer With High-Frequency Signal Injection for Synchronous Reluctance Motor Drives

Year: 2014

Version: Post print

Please cite the original version:

Tuovinen, Toni & Hinkkanen, Marko. 2014. Adaptive Full-Order Observer With High-Frequency Signal Injection for Synchronous Reluctance Motor Drives. IEEE Journal of Emerging and Selected Topics in Power Electronics. Volume 2, Issue 2. 9. DOI: 10.1109/jestpe.2013.2294359.

Adaptive Full-Order Observer with High-Frequency Signal Injection for Synchronous Reluctance Motor Drives

Toni Tuovinen and Marko Hinkkanen

Aalto University School of Electrical Engineering
P.O. Box 13000, FI-00076 Aalto, Finland

***Abstract*—A back-EMF-based position observer for motion-sensorless synchronous reluctance motor drives is augmented with high-frequency signal-injection method for improved low-speed operation. Previously proposed observer structure is further improved to account for the cross saturation in the motor. The combined observer is experimentally evaluated using a 6.7-kW synchronous reluctance motor drive in low-speed operation and under various load conditions. The resulting position error at low speeds and standstill is small.**

***Index Terms*—Observer, parameter uncertainties, speed sensorless, stability conditions.**

I. Introduction

Synchronous reluctance motor (SyRM) has recently reemerged as a contender to the induction motor in variable-speed drives [1]–[3]. As compared to the permanent-magnet synchronous motor (PMSM), the SyRM is magnetized from the stator winding, which renders field-weakening operation a straightforward procedure. The recent price increase of rare-earth metals has also made the SyRM and permanent-magnet assisted SyRM more favorable in relation to the PMSM.

Position-sensorless operation is commonly preferred. At high speeds, methods based on the back electromotive force (EMF) can be used. Since the SyRM can be seen as a special case of the salient PMSM, back-EMF-based methods suitable for salient PMSMs, for example the observers proposed in [4], [5], can be used for SyRMs with slight modifications.

The back-EMF-based methods fail to estimate the position at low speeds and standstill. As the SyRM is inherently salient, methods for accurate rotor-position estimation even at standstill are readily applicable. These methods can be roughly categorized as

- signal-injection methods [2], [6]–[9]
- modified PWM [10], [11]
- methods based on stator current variation without additional signal [12], [13].

Although some authors favor the usage of signal-injection methods at all speeds [14], it is often desirable to avoid additional noise and losses by using a back-EMF-based position estimation method, combined with a signal-injection method applied only at the lowest speeds [2], [15], [16].

SyRMs are usually magnetically saturated in the rated operating point. The d-axis flux component saturates strongly as a function of the corresponding current component. Furthermore, the d-axis saturation is coupled with the q-axis saturation. This cross saturation presents an error in the position estimate obtained from the signal-injection method, but the cross saturation is usually omitted.

In this paper, an adaptive full-order observer, combined with high-frequency signal injection [4], is applied for a SyRM drive in order to improve low-speed operation. The method is further improved to account for the cross saturation in the motor. A minimum requirement for any observer is that the estimation-error dynamics of the closed-loop system are locally stable at every operating point in ideal conditions. In order to satisfy this requirement and to simplify the tuning procedure, a stabilizing gain proposed in [17] is taken as a starting point. This gain is modified in order to take into account the effect of the signal-injection method on the estimation-error dynamics.

After a review of the motor model in Section II, and the rotor-position observers in Section III, the main contributions of the paper are presented Section IV:

1) A modified position estimation method, based on signal injection, which reduces the steady-state estimation error caused by cross saturation, is proposed.
2) A stabilizing gain modification for the combined observer is proposed.

The experimental setup is described in Section V, and the performance of the drive at low speeds and standstill is experimentally validated using a 6.7-kW SyRM drive in Section VI.

II. SyRM Model

A. Fundamental-Excitation Model

Real space vectors will be used here. For example, the stator-current vector is $\boldsymbol{i}_\mathrm{s} = [i_\mathrm{d}, i_\mathrm{q}]^\mathrm{T}$, where i_d and i_q are the components of the vector and the matrix transpose is marked with the superscript T. The orthogonal rotation matrix is defined as

$$\mathbf{J} = \begin{bmatrix} 0 & -1 \\ 1 & 0 \end{bmatrix}.$$

The electrical position of the d-axis is denoted by ϑ_m. The d-axis is defined as the direction of the maximum inductance of the rotor. The position depends on the electrical angular rotor speed ω_m according to

$$\frac{\mathrm{d}\vartheta_\mathrm{m}}{\mathrm{d}t} = \omega_\mathrm{m} \tag{1a}$$

To simplify the analysis in the following sections, the machine model will be expressed in the *estimated* rotor reference frame, whose d-axis is aligned at $\hat{\vartheta}_\mathrm{m}$ with respect to the stator reference frame. The stator inductance is

$$\boldsymbol{L} = \mathrm{e}^{-\tilde{\vartheta}_\mathrm{m}\mathbf{J}} \begin{bmatrix} L_\mathrm{d} & 0 \\ 0 & L_\mathrm{q} \end{bmatrix} \mathrm{e}^{\tilde{\vartheta}_\mathrm{m}\mathbf{J}} \tag{1b}$$

where $\tilde{\vartheta}_\mathrm{m} = \hat{\vartheta}_\mathrm{m} - \vartheta_\mathrm{m}$ is the estimation error in the rotor position, L_d the direct-axis inductance, and L_q the quadrature-axis inductance. The voltage equation is

$$\frac{\mathrm{d}\boldsymbol{\psi}_\mathrm{s}}{\mathrm{d}t} = \boldsymbol{u}_\mathrm{s} - R_\mathrm{s}\boldsymbol{i}_\mathrm{s} - \hat{\omega}_\mathrm{m}\mathbf{J}\boldsymbol{\psi}_\mathrm{s} \tag{1c}$$

where $\boldsymbol{\psi}_\mathrm{s}$ is the stator-flux vector, $\boldsymbol{u}_\mathrm{s}$ the stator-voltage vector, R_s the stator resistance, and $\hat{\omega}_\mathrm{m} = \mathrm{d}\hat{\vartheta}_\mathrm{m}/\mathrm{d}t$ is the angular speed of the coordinate system. The stator current is a non-linear function

$$\boldsymbol{i}_\mathrm{s} = \boldsymbol{L}^{-1}\boldsymbol{\psi}_\mathrm{s} \tag{1d}$$

of the stator-flux vector and the position error $\tilde{\vartheta}_\mathrm{m}$.

The magnetic saturation has been modeled as functions of the estimated flux [18],

$$i_\mathrm{d} = \frac{\psi_\mathrm{d}}{L_\mathrm{du}}\left(1 + \alpha|\psi_\mathrm{d}|^a + \frac{\delta L_\mathrm{du}}{d+2}|\psi_\mathrm{d}|^c|\psi_\mathrm{q}|^{d+2}\right) \tag{2a}$$

$$i_\mathrm{q} = \frac{\psi_\mathrm{q}}{L_\mathrm{qu}}\left(1 + \gamma|\psi_\mathrm{q}|^b + \frac{\delta L_\mathrm{qu}}{c+2}|\psi_\mathrm{d}|^{c+2}|\psi_\mathrm{q}|^d\right) \tag{2b}$$

where all parameters should be positive.

B. High-Frequency Model

The incremental inductances seen by the high-frequency excitation are

$$L_\mathrm{dd} = \frac{\partial\psi_\mathrm{d}}{\partial i_\mathrm{d}}, \quad L_\mathrm{dq} = \frac{\partial\psi_\mathrm{d}}{\partial i_\mathrm{q}}, \quad L_\mathrm{qd} = \frac{\partial\psi_\mathrm{q}}{\partial i_\mathrm{d}}, \quad L_\mathrm{qq} = \frac{\partial\psi_\mathrm{q}}{\partial i_\mathrm{q}} \tag{3}$$

Due to reciprocity, it is assumed that $L_\mathrm{qd} = L_\mathrm{dq}$.

It is worth noticing that the incremental inductances seen by the high-frequency excitation do not necessarily coincide with the incremental inductances seen by the fundamental excitation [8]. This is demonstrated in Fig. 1, where measured incremental inductances and incremental inductances predicted by the fundamental-excitation model (2) are depicted for a 6.7-kW SyRM (see Section V). In Fig. 1(a), L_dd is shown as a function of i_d for two different values of i_q. In Figs. 1(b) and 1(c), L_qq and L_dq are shown as functions of i_q for two different values of i_d, respectively. It can be seen that L_dd and L_dq estimated by the fundamental-excitation model (lines) differs considerably from the measured values (crosses and circles), but the estimated L_qq coincides with the measured values with good accuracy.

III. Rotor-Position Observers

A. Adaptive Full-Order Observer

In the adaptive full-order observer [4], [19], the stator-flux vector is estimated according to

$$\frac{\mathrm{d}\hat{\boldsymbol{\psi}}_\mathrm{s}}{\mathrm{d}t} = \boldsymbol{u}_\mathrm{s} - \hat{R}_\mathrm{s}\hat{\boldsymbol{i}}_\mathrm{s} - \hat{\omega}_\mathrm{m}\mathbf{J}\hat{\boldsymbol{\psi}}_\mathrm{s} + \boldsymbol{K}\tilde{\boldsymbol{i}}_\mathrm{s} \tag{4a}$$

$$\hat{\boldsymbol{i}}_\mathrm{s} = \hat{\boldsymbol{L}}^{-1}\hat{\boldsymbol{\psi}}_\mathrm{s} \tag{4b}$$

where $\hat{\boldsymbol{i}}_\mathrm{s}$ is the estimated stator-current vector, $\tilde{\boldsymbol{i}}_\mathrm{s} = \hat{\boldsymbol{i}}_\mathrm{s} - \boldsymbol{i}_\mathrm{s}$ is the estimation error of the stator current, $\boldsymbol{K}$ is the gain matrix, and $\hat{R}_\mathrm{s}$ is the estimated stator resistance. The gain matrix is [17]

$$\boldsymbol{K} = \begin{bmatrix} \hat{R}_\mathrm{s} + \hat{L}_\mathrm{d}k_1 & -\hat{L}_\mathrm{q}\hat{\beta}k_1 \\ \hat{L}_\mathrm{d}k_2 & \hat{R}_\mathrm{s} - \hat{L}_\mathrm{q}\hat{\beta}k_2 \end{bmatrix} \tag{5a}$$

where $\hat{L}_\mathrm{d}$ and $\hat{L}_\mathrm{q}$ are the estimated d and q axis inductances, respectively, $\beta = i_\mathrm{q}/i_\mathrm{d}$, and k_1 and k_2 are given by

$$k_1 = -\frac{b + \beta(c/\hat{\omega}_\mathrm{m} - \hat{\omega}_\mathrm{m})}{\beta^2 + 1}, \quad k_2 = \frac{\beta b - c/\hat{\omega}_\mathrm{m} + \hat{\omega}_\mathrm{m}}{\beta^2 + 1} \tag{5b}$$

where b and c should be positive.

The rotor speed is estimated with the PI mechanism

$$\hat{\omega}_\mathrm{m} = \boldsymbol{k}_\mathrm{p}\tilde{\boldsymbol{i}}_\mathrm{s} + \boldsymbol{k}_\mathrm{i}\int\tilde{\boldsymbol{i}}_\mathrm{s}\mathrm{d}t \tag{6}$$

The gain vectors $\boldsymbol{k}_\mathrm{p}$ and $\boldsymbol{k}_\mathrm{i}$ are chosen to utilize the estimation error only in the q axis direction,

$$\boldsymbol{k}_\mathrm{p} = [0, k_\mathrm{p}], \quad \boldsymbol{k}_\mathrm{i} = [0, k_\mathrm{i}] \tag{7}$$

For convenience, the gains k_p and k_i are selected according to

$$k_\mathrm{p} = \frac{\hat{L}_\mathrm{q}d}{(\hat{L}_\mathrm{d} - \hat{L}_\mathrm{q})i_\mathrm{d}}, \quad k_\mathrm{i} = \frac{\hat{L}_\mathrm{q}e}{(\hat{L}_\mathrm{d} - \hat{L}_\mathrm{q})i_\mathrm{d}} \tag{8}$$

where d and e are design parameters, which may depend on the rotor speed. With this gain selection, the characteristic polynomial of the closed-loop system consisting of (1) and (4) – (8) can, after linearization, be split into a product of two second-order polynomials,

$$(s^2 + bs + c)(s^2 + ds + e) \tag{9}$$

and the stability is guaranteed for all positive values of b, c, d, and e, if the parameter estimates are accurate. The observer is of the fourth order, and there are four gains. In order to reduce the number of design parameters, d and e can be chosen as [20]

$$d = 2\rho, \quad e = \rho^2 \tag{10}$$

yielding double pole located at $s = -\rho$. The remaining three design parameters are b, c, and ρ, which should be positive.

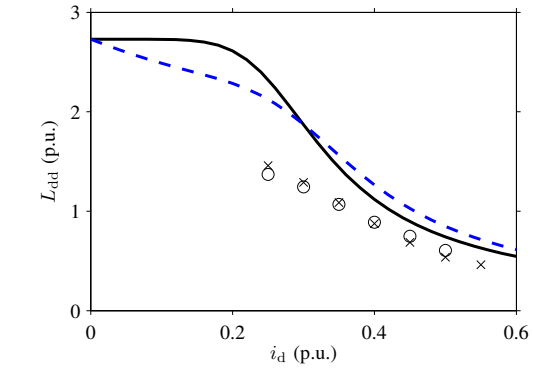

(a)

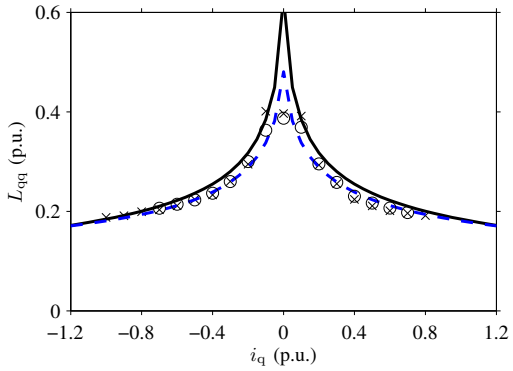

(b)

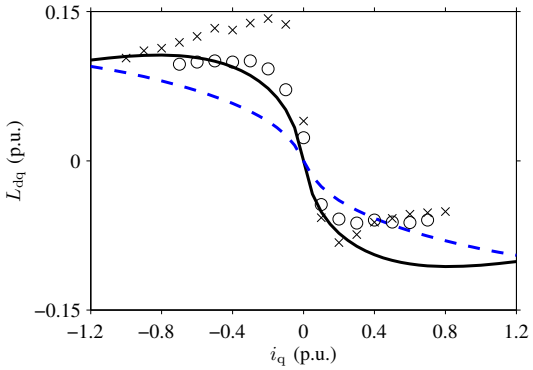

(c)

Fig. 1. Incremental inductances as functions of currents for a 6.7-kW SyRM: (a) L_{dd} as function of i_{d} for two different values of i_{q}, (b) L_{qq} as function of i_{q} for two different values of i_{d}, (c) L_{dq} as function of i_{q} for two different values of i_{d}. In (a), the values of i_{q} are 0 p.u. (solid line, crosses) and 0.75 p.u. (dashed line, circles). In (b) and (c), the values of i_{d} are 0.3 p.u. (solid line, crosses) and 0.5 p.u. (dashed line, circles). Crosses and circles are measured values, lines are values estimated by the fundamental-excitation model (2).

B. High-Frequency Signal Injection

A high-frequency voltage excitation is superimposed on the stator voltage in the estimated d-axis direction [14],

$$\boldsymbol{u}_{\mathrm{c}} = \begin{bmatrix} u_{\mathrm{c}} \cos(\omega_{\mathrm{c}} t) \\ 0 \end{bmatrix}. \tag{11}$$

The high-frequency current responses depend on the position error,

$$i_{\mathrm{dc}} = \frac{u_{\mathrm{c}} \sin(\omega_{\mathrm{c}} t)}{\omega_{\mathrm{c}} L_{\mathrm{det}}} \left[L_{\Sigma} - L_{\Delta} \cos(2\tilde{\vartheta}_{\mathrm{m}}) - L_{\mathrm{dq}} \sin(2\tilde{\vartheta}_{\mathrm{m}}) \right] \tag{12a}$$

$$i_{\mathrm{qc}} = \frac{u_{\mathrm{c}} \sin(\omega_{\mathrm{c}} t)}{\omega_{\mathrm{c}} L_{\mathrm{det}}} \left[L_{\Delta} \sin(2\tilde{\vartheta}_{\mathrm{m}}) - L_{\mathrm{dq}} \cos(2\tilde{\vartheta}_{\mathrm{m}}) \right] \tag{12b}$$

where

$$L_{\mathrm{det}} = L_{\mathrm{dd}} L_{\mathrm{qq}} - L_{\mathrm{dq}}^2 \tag{13a}$$

$$L_{\Sigma} = \frac{L_{\mathrm{dd}} + L_{\mathrm{qq}}}{2} \tag{13b}$$

$$L_{\Delta} = \frac{L_{\mathrm{dd}} - L_{\mathrm{qq}}}{2} \tag{13c}$$

Conventionally, only the high-frequency current component perpendicular to the injected signal is used in the position estimation, which is then demodulated and low-pass filtered (LPF) [20], [21],

$$\begin{aligned} \epsilon &= \mathrm{LPF}\left\{ i_{\mathrm{q}} \sin(\omega_{\mathrm{c}} t) \right\} \\ &= \frac{u_{\mathrm{c}}}{2\omega_c L_{\mathrm{det}}} \left[L_{\Delta} \sin(2\tilde{\vartheta}_{\mathrm{m}}) - L_{\mathrm{dq}} \cos(2\tilde{\vartheta}_{\mathrm{m}}) \right] \end{aligned} \tag{14}$$

This error signal ϵ is then fed to the PI mechanism

$$\omega_{\epsilon} = \gamma_{\mathrm{p}} \epsilon + \gamma_{\mathrm{i}} \int \epsilon \mathrm{d}t. \tag{15}$$

The gains are

$$\gamma_{\mathrm{p}} = \frac{\alpha_{\mathrm{i}}}{2k_{\epsilon}}, \quad \gamma_{\mathrm{i}} = \frac{\alpha_{\mathrm{i}}^2}{6k_{\epsilon}}, \tag{16}$$

where α_{i} is the approximate bandwidth of the PI mechanism, k_{ϵ} is the signal-injection gain given by

$$k_{\epsilon} = \frac{u_{\mathrm{c}}}{\omega_{\mathrm{c}}} \frac{L_{\mathrm{d}} - L_{\mathrm{q}}}{4 L_{\mathrm{d}} L_{\mathrm{q}}}, \tag{17}$$

and the bandwidth of the low-pass filter in (14) is $\alpha_{\mathrm{lp}} = 3\alpha_{\mathrm{i}}$ [4].

A smooth transition from standstill to high-speed operation is implemented by decreasing the injected voltage and the bandwidth of the PI mechanism as the speed increases,

$$u_{\mathrm{c}} = u_{\mathrm{c0}} f(\hat{\omega}_{\mathrm{m}}), \quad \alpha_{\mathrm{i}} = \alpha_{\mathrm{i0}} f(\hat{\omega}_{\mathrm{m}}) \tag{18}$$

where the transition function is selected as

$$f(\hat{\omega}_{\mathrm{m}}) = \begin{cases} 1 - \left| \frac{\hat{\omega}_{\mathrm{m}}}{\omega_{\Delta}} \right|, & \text{if } |\hat{\omega}_{\mathrm{m}}| \leq \omega_{\Delta} \\ 0, & \text{otherwise.} \end{cases} \tag{19}$$

The correction ω_{ϵ} is combined with the observer (4), resulting in

$$\frac{\mathrm{d}\hat{\boldsymbol{\psi}}_{\mathrm{s}}}{\mathrm{d}t} = \boldsymbol{u}_{\mathrm{s}} - \hat{R}_{\mathrm{s}} \hat{\boldsymbol{i}}_{\mathrm{s}} - (\hat{\omega}_{\mathrm{m}} + \omega_{\epsilon}) \mathbf{J} \hat{\boldsymbol{\psi}}_{\mathrm{s}} + \boldsymbol{K} \tilde{\boldsymbol{i}}_{\mathrm{s}} \tag{20}$$

Due to cross saturation, this scheme leads to a steady-state position error [22]

$$\tilde{\vartheta}_{\mathrm{m0}} = \frac{1}{2} \arctan\left(\frac{L_{\mathrm{dq}}}{L_{\Delta}} \right). \tag{21}$$

IV. Proposed Scheme

A. Proposed Error Signal

The proposed method is to use a combination of the d and q axis current components, which is demodulated and low-pass filtered,

$$\begin{aligned}\epsilon &= \mathrm{LPF}\left\{\left(\frac{\hat{L}_{\mathrm{dq}}}{\hat{L}_{\mathrm{qq}}}i_{\mathrm{d}}+i_{\mathrm{q}}\right)\sin(\omega_{\mathrm{c}}t)\right\}\\ &= \frac{u_{\mathrm{c}}}{\omega_c L_{\mathrm{det}}\hat{L}_{\mathrm{qq}}}\left(L_{\mathrm{dq}}\hat{L}_{\mathrm{qq}}+\hat{L}_{\mathrm{dq}}L_{\Delta}\right)\sin^2\tilde{\vartheta}_{\mathrm{m}}\\ &+ \frac{u_{\mathrm{c}}}{2\omega_c L_{\mathrm{det}}\hat{L}_{\mathrm{qq}}}\left(L_{\Delta}\hat{L}_{\mathrm{qq}}-L_{\mathrm{dq}}\hat{L}_{\mathrm{dq}}\right)\sin(2\tilde{\vartheta}_{\mathrm{m}})\\ &+ \frac{u_{\mathrm{c}}}{2\omega_c L_{\mathrm{det}}\hat{L}_{\mathrm{qq}}}\left(L_{\mathrm{qq}}\hat{L}_{\mathrm{dq}}-L_{\mathrm{dq}}\hat{L}_{\mathrm{qq}}\right).\end{aligned} \tag{22}$$

where $\hat{L}_{\mathrm{dq}}$ is the estimated incremental inductance between the two axis and $\hat{L}_{\mathrm{qq}}$ is the estimated q-axis incremental inductance. The ratio $\hat{L}_{\mathrm{dq}}/\hat{L}_{\mathrm{qq}}$ can be regarded as a compensation factor, which can also include model and implementation uncertainties, such as system delays, for example. It can be seen from Fig. 1(c) that $\hat{L}_{\mathrm{dq}}/\hat{L}_{\mathrm{qq}} > 0$, if $i_{\mathrm{q}} < 0$ and $\hat{L}_{\mathrm{dq}}/\hat{L}_{\mathrm{qq}} < 0$, if $i_{\mathrm{q}} > 0$.

Assuming accurate parameter estimates and omitting the term proportional to $\sin^2\tilde{\vartheta}_{\mathrm{m}}$, the error signal is

$$\epsilon \approx \frac{u_{\mathrm{c}}}{2\omega_c L_{\mathrm{det}}L_{\mathrm{qq}}}\left(L_{\Delta}L_{\mathrm{qq}}-L_{\mathrm{dq}}^2\right)\sin(2\tilde{\vartheta}_{\mathrm{m}}) \tag{23}$$

which vanishes with $\tilde{\vartheta}_{\mathrm{m}} = 0$. In this case, the signal-injection gain is

$$k_{\epsilon} = \frac{u_{\mathrm{c}}}{\omega_{\mathrm{c}}}\frac{L_{\Delta}L_{\mathrm{qq}}-L_{\mathrm{dq}}^2}{2L_{\mathrm{det}}L_{\mathrm{qq}}}, \tag{24}$$

which reduces to (17), if $L_{\mathrm{dq}} = 0$.

The method is closely related to the method proposed in [2], which is based on tracking the flux variations in the estimated q-axis direction. However, the scheme in [2] requires relatively high-amplitude carrier voltage signal, and the stability analysis has been omitted.

B. Proposed Gain Selection

Analytical and numerical studies indicated that the gain selection (5) with $b > 0$ and $c > 0$, based on the studies for the adaptive full-order observer in [17], is insufficient for the combined observer near standstill in the regenerating mode, since the signal-injection correction ω_{ϵ} in (20) affects the estimation-error dynamics. Experimental evaluations and numerical analysis indicated that it is sufficient to introduce two new gains to the gain matrix (5a),

$$\boldsymbol{K} = \begin{bmatrix}\hat{R}_{\mathrm{s}}+\hat{L}_{\mathrm{d}}[k_1-k_3 f(\hat{\omega}_{\mathrm{m}})] & -\hat{L}_{\mathrm{q}}\hat{\beta}k_1\\ \hat{L}_{\mathrm{d}}[k_2+k_4\beta f(\hat{\omega}_{\mathrm{m}})] & \hat{R}_{\mathrm{s}}-\hat{L}_{\mathrm{q}}\hat{\beta}k_2\end{bmatrix} \tag{25}$$

where k_3 and k_4 should be positive. This can be also interpreted as replacing the observer parameters b and $c/\hat{\omega}_{\mathrm{m}}$ in (5b) with parameters b_1 and c_1, which now are not necessarily positive,

$$b_1 = b+(k_4\beta^2+k_3)f(\hat{\omega}_{\mathrm{m}}), \quad c_1 = \frac{c}{\hat{\omega}_{\mathrm{m}}}+\beta(k_3-k_4)f(\hat{\omega}_{\mathrm{m}}). \tag{26}$$

It can be seen that in the regenerating mode at near zero speed c_1 can become negative, while b_1 remains positive.

The robustness of the combined observer is studied with the negative rated load and with the rated load, with actual parameters L_{d} = 2.00 p.u., L_{q} = 0.3 p.u., and R_{s} = 0.042 p.u. of the 6.7-kW SyRM. Other parameters were: $\rho = 2$ p.u., $u_{\mathrm{c0}} = 0.1$ p.u., $\omega_{\mathrm{c}} = 2\pi\cdot 500$ rad/s, $\omega_{\Delta} = 0.1$ p.u., and $\alpha_{\mathrm{i0}} = 0.1$ p.u. The same relative uncertainty (10%) is assumed for all three model parameters $\hat{L}_{\mathrm{d}}$, $\hat{L}_{\mathrm{q}}$, and $\hat{R}_{\mathrm{s}}$. Hence, eight different worst-case combinations, consisting of minimum and maximum values of the model parameters, can be formed. For example, one of the worst-case combinations is $\hat{L}_{\mathrm{d}} = 0.9L_{\mathrm{d}}$, $\hat{L}_{\mathrm{q}} = 1.1L_{\mathrm{q}}$, and $\hat{R}_{\mathrm{s}} = 0.9R_{\mathrm{s}}$. At each studied operating point, the local stability of the system was analyzed for all eight worst-case combinations of erroneous model parameters.

The stability of the estimation-error dynamics with erroneous model parameters was analyzed for different values of the design parameters b and c. The stability maps are depicted in Fig. 2, where stable areas are shaded and unstable areas are blank. Fig. 2(a) shows the stability map in the design-parameter space for $i_{\mathrm{q}} = -1$ p.u. Fig. 2(b) shows the stability map in the design-parameter space for $i_{\mathrm{q}} = 1$ p.u. It can be seen that the shape of the stable region is drastically changed with varying load, and that there are no stable points for $c > 0$, when $i_{\mathrm{q}} = -1$ p.u. for this particular case. It is worth noticing that the combined observer is more robust when applied for PMSM drives, since the stability is governed by the operation-point parameter β, which for PMSMs is [17]

$$\beta = \frac{(L_{\mathrm{d}}-L_{\mathrm{q}})i_{\mathrm{q}}}{\psi_{\mathrm{pm}}+(L_{\mathrm{d}}-L_{\mathrm{q}})i_{\mathrm{d}}}$$

where ψ_{pm} is the PM-flux. For PMSMs, the parameter β does not change as drastically as it does for SYRMs when the load is varied.

V. Experimental Setup and Parameters

The motion-sensorless control system was implemented in a dSPACE DS1104 PPC/DSP board. A 6.7-kW four-pole SyRM was fed by a frequency converter that is controlled by the DS1104 board. The rated values of the SyRM are: speed 3175 r/min; frequency 105.8 Hz; line-to-line rms voltage 370 V; rms current 15.5 A; and torque 20.1 Nm. The base values for angular speed, voltage, and current are defined as $2\pi\cdot 105.8$ rad/s, $\sqrt{2/3}\cdot 370$ V, and $\sqrt{2}\cdot 15.5$ A, respectively.

A servo motor was used as a loading machine. The rotor speed ω_{m} and position ϑ_{m} were measured using an incremental encoder for monitoring purposes. The total moment of inertia of the experimental setup is 0.015 kgm^2 (2.7 times the inertia of the SyRM rotor).

The stator currents and the DC-link voltage were measured, and the reference voltage obtained from the current controller

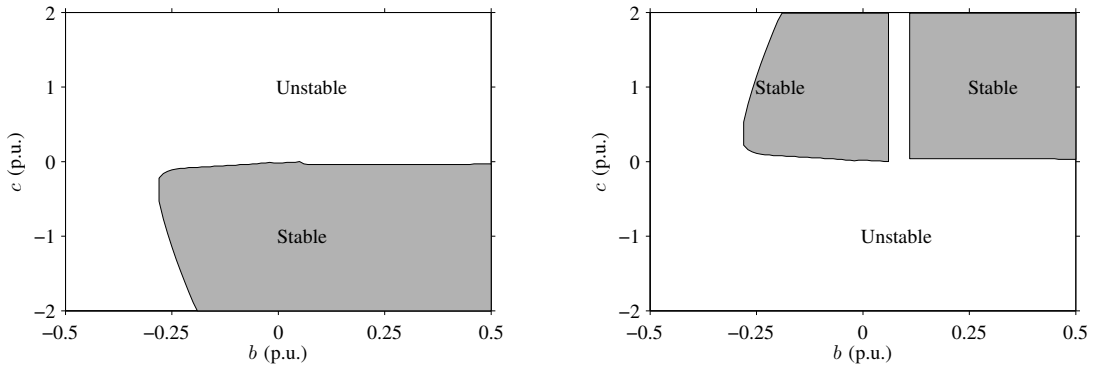

Fig. 2. Stability maps in the design parameter space for 10% parameter uncertainties: (a) $i_\mathrm{q} = -1$ p.u., and (b) $i_\mathrm{q} = 1$ p.u. The d-axis current is $i_\mathrm{d} = 0.5$ p.u. and $\hat{\omega}_\mathrm{m} = 0$. Stable areas are shaded, and unstable areas are blank.

TABLE I
PER-UNIT PARAMETERS FOR SATURATION MODEL

L_du	L_qu	α	γ	δ	a	b	c	d
2.73	0.843	0.333	5.58	2.60	6.6	0.8	1	0

was used for the observer. The sampling was synchronized to the modulation, and both the switching frequency and the sampling frequency were 5 kHz. A simple current feedforward compensation for dead times and power device voltage drops was applied.

The control system was augmented with a speed controller, whose feedback signal was the speed estimate $\hat{\omega}_\mathrm{m}$ obtained from the proposed observer. The bandwidth of this PI controller, including active damping [23], was $2\pi \cdot 5.3$ rad/s (0.05 p.u.). The gain values were chosen based on empirical results: $b = 0.05$, $c = 0.1|\hat{\omega}_\mathrm{m}|$, $k_3 = 0.04$, $k_4 = 0.2$, and $\rho = 2$ p.u. The parameters for the signal injection were: $u_\mathrm{c0} = 0.1$ p.u., $\omega_\mathrm{c} = 2\pi \cdot 500$ rad/s, $\omega_\Delta = 0.1$ p.u., and $\alpha_\mathrm{i0} = 0.1$ p.u. The stator resistance estimate is $\hat{R}_\mathrm{s} = 0.042$ p.u. The saturation model parameters are given in Table I [18]. Since at low speeds even small parameter errors may result in considerable errors in the estimated fluxes, the saturation model is implemented using the measured current components as independent variables. Then, another estimates for $\hat{\psi}_\mathrm{d}$ and $\hat{\psi}_\mathrm{q}$ are searched iteratively so that the estimation errors $\hat{i}_\mathrm{d} - i_\mathrm{d}$ and $\hat{i}_\mathrm{q} - i_\mathrm{q}$ vanish.

VI. EXPERIMENTAL RESULTS

Experimental results of a sloped speed reversal from $\hat{\omega}_\mathrm{m} = 0.1$ p.u. to $\hat{\omega}_\mathrm{m} = -0.1$ p.u. and back to 0.1 p.u. with negative rated load torque applied using only the q-axis component of the high-frequency current ($L_\mathrm{dq}/L_\mathrm{qq} = 0$) are depicted in Fig. 3(a). It can be seen that the position error is large, and the system is unstable at some operation points.

Similar results for a constant compensation, $L_\mathrm{dq}/L_\mathrm{qq} = -0.4\mathrm{sgn}(i_\mathrm{q})$, are depicted in Fig. 3(b). It can be seen that the mean position error is close to zero, and the noise in the estimation error is smaller. Since the test is carried out with constant load, a constant compensation has been used. Experiments indicated that, in this particular test, the drive becomes unstable, if the error in $\hat{R}_\mathrm{s}$ is larger than approximately $\pm 10\%$.

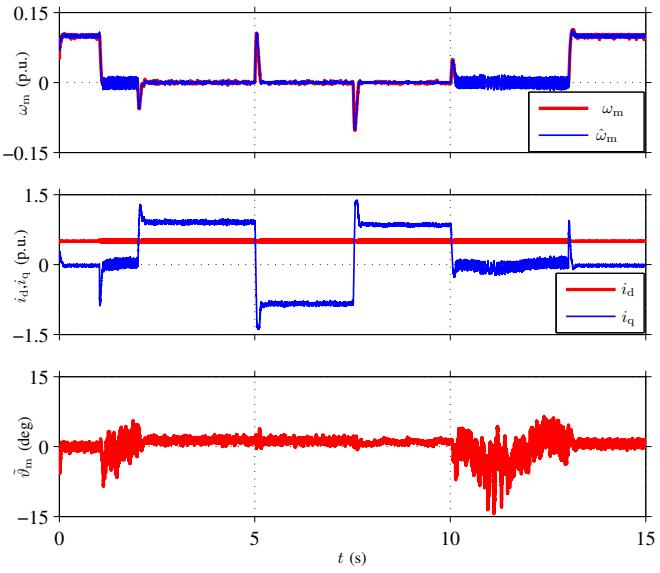

Fig. 4. Experimental results showing load-torque steps (0 → rated → −rated → rated → 0) when the speed reference is kept at 0. The d-axis current is 0.5 p.u., and $L_\mathrm{dq}/L_\mathrm{qq} = -0.4\mathrm{sgn}(i_\mathrm{q})$.

Experimental results of load-torque steps when the speed reference was kept at 0 are shown in Fig. 4. The load torque was stepped to the rated load torque at $t = 2.0$ s, reversed at $t = 5.0$ s, reversed again at $t = 7.5$ s and removed at $t = 10$ s. It can be seen that the combined observer behaves well in load transients in standstill operation. The compensation factor is chosen as $L_\mathrm{dq}/L_\mathrm{qq} = -0.4\mathrm{sgn}(i_\mathrm{q})$, which is tuned for the rated load operation with $i_\mathrm{d} = 0.5$ p.u. In no load operation, this type of function results in oscillations, as can be seen from Fig. 4.

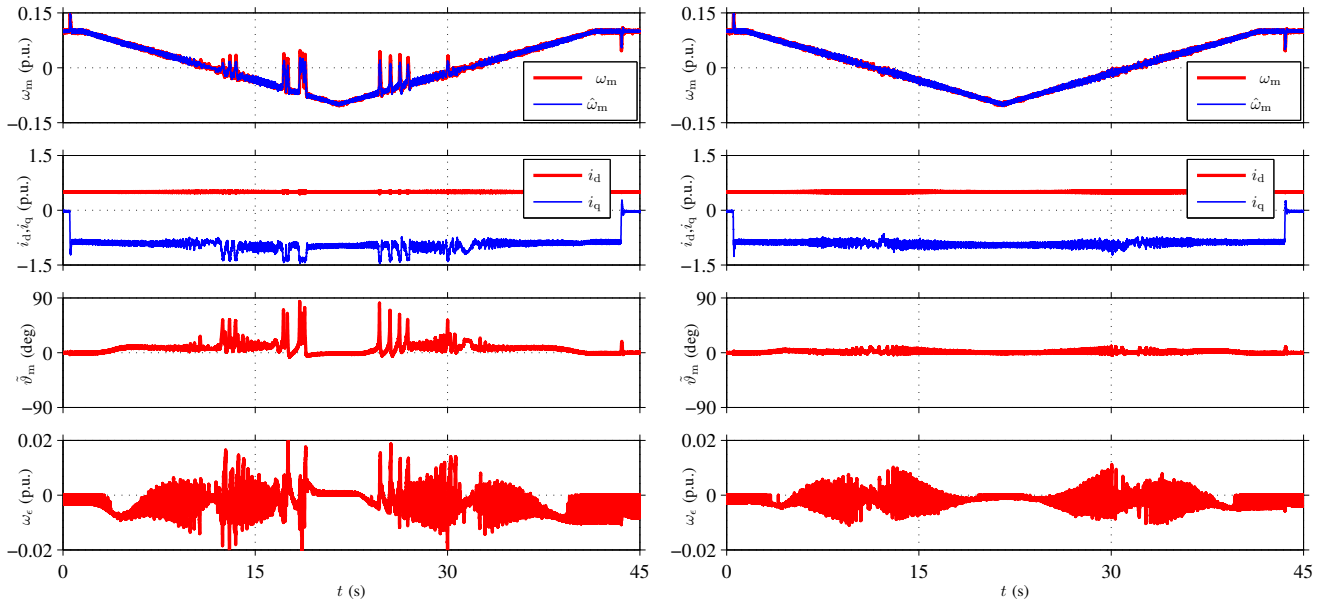

Fig. 3. Experimental results of a sloped speed reversal (0.1 p.u. $\rightarrow -0.1$ p.u. $\rightarrow$ 0.1 p.u.) with negative rated load torque applied. The d-axis current is 0.5 p.u., and the compensation for the cross saturation is: (a) $L_\mathrm{dq}/L_\mathrm{qq} = 0$, (b) $L_\mathrm{dq}/L_\mathrm{qq} = -0.4\mathrm{sgn}(i_\mathrm{q})$.

VII. Conclusions

In this paper, an adaptive full-order observer with signal injection is implemented and improved for SyRM drives. The evaluated scheme demonstrates good performance and small position error in laboratory experiments, but is relatively sensitive to the parameter errors of the fundamental-excitation model. This suggests that the scheme could be further improved with a stator-resistance adaptation mechanism, for example.

Acknowledgment

The authors gratefully acknowledge ABB Oy for the financial support.

References

[1] R. Lagerquist, I. Boldea, and J. Miller, "Sensorless control of the synchronous reluctance motor," *IEEE Trans. Ind. Appl.*, vol. 30, no. 3, pp. 673–682, May/June 1994.

[2] E. Capecchi, P. Guglielmo, M. Pastorelli, and A. Vagati, "Position-sensorless control of the transverse-laminated synchronous reluctance motor," *IEEE Trans. Ind. Appl.*, vol. 37, no. 6, pp. 1768–1776, Nov./Dec. 2001.

[3] H. F. Hofmann, S. R. Sanders, and A. EL-Antably, "Stator-flux-oriented vector control of synchronous reluctance machines with maximized efficiency," *IEEE Trans. Ind. Electron.*, vol. 51, no. 5, pp. 1066–1072, Oct. 2004.

[4] A. Piippo, M. Hinkkanen, and J. Luomi, "Analysis of an adaptive observer for sensorless control of interior permanent magnet synchronous motors," *IEEE Trans. Ind. Electron.*, vol. 55, no. 2, pp. 570–576, Feb. 2008.

[5] M. Hinkkanen, T. Tuovinen, L. Harnefors, and J. Luomi, "A combined position and stator-resistance observer for salient PMSM drives: design and stability analysis," *IEEE Trans. Power Electron.*, vol. 27, no. 2, pp. 601–609, Feb. 2012.

[6] J.-I. Ha, S.-J. Kang, and S.-K. Sul, "Position-controlled synchronous reluctance motor without rotational transducer," *IEEE Trans. Ind. Appl.*, vol. 35, no. 6, pp. 1393–1398, Nov./Dec. 1999.

[7] A. Consoli, F. Russo, G. Scarcella, and A. Testa, "Low- and zero-speed sensorless control of synchronous reluctance motors," *Electr. Power Comp. Syst.*, vol. 35, no. 5, pp. 1050–1057, Sep./Oct. 1999.

[8] H. W. de Kock, M. J. Kamper, O. C. Ferreira, and R. M. Kennel, "Position sensorless control of the reluctance synchronous machine considering high frequency inductances," in *Proc. PEDS 2007*, Bangkok, Thailand, Nov. 2007, pp. 812–821.

[9] S.-C. Agarlită, I. Boldea, and F. Blaabjerg, "High-frequency-injection-assisted "active flux"-based sensorless vector control of reluctance synchronous motors, with experiments from zero speed," *IEEE Trans. Ind. Appl.*, vol. 48, no. 6, pp. 1931–1939, Nov./Dec. 2012.

[10] M. Schroedl and P. Weinmeier, "Sensorless control of reluctance machines at arbitrary operating conditions including standstill," *IEEE Trans. Power Electron.*, vol. 9, no. 2, pp. 225–231, Mar. 1994.

[11] R. Morales-Caporal and M. Pacas, "Encoderless predictive direct torque control for synchronous reluctance machines at very low and zero speed," *IEEE Trans. Ind. Electron.*, vol. 55, no. 12, pp. 4408–4416, Dec. 2008.

[12] T. Matsuo and T. A. Lipo, "Rotor position detection scheme for synchronous reluctance motor based on current measurements," *IEEE Trans. Ind. Appl.*, vol. 31, no. 4, pp. 860–868, July/Aug. 1995.

[13] M.-Y. Wei and T.-H. Liu, "A high-performance sensorless position control system of a synchronous reluctance motor using dual current-slope estimating technique," *IEEE Trans. Ind. Electron.*, vol. 59, no. 9, pp. 3411–3426, Sept. 2012.

[14] M. J. Corley and R. D. Lorenz, "Rotor position and velocity estimation for a salient-pole permanent magnet synchronous machine at standstill and high speeds," *IEEE Trans. Ind. Appl.*, vol. 34, no. 4, pp. 784–789, Jul./Aug. 1998.

[15] O. Wallmark, L. Harnefors, and O. Carlson, "An improved speed and position estimator for salient permanent-magnet synchronous motors," *IEEE Trans. Ind. Electron.*, vol. 52, no. 1, pp. 255–262, Feb. 2005.

[16] W. Hammel and R. M. Kennel, "Position sensorless control of PMSM by synchronous injection and demodulation of alternating carrier voltage," in *Proc. IEEE SLED 2010*, Padova, Italy, July 2010, pp. 56–63.

[17] T. Tuovinen, M. Hinkkanen, L. Harnefors, and J. Luomi, "Comparison of a reduced-order observer and a full-order observer for sensorless synchronous motor drives," *IEEE Trans. Ind. Appl.*, vol. 48, no. 6, pp. 1959–1967, Nov./Dec. 2012.

[18] Z. Qu, T. Tuovinen, and M. Hinkkanen, "Inclusion of magnetic satu-

ration in dynamic models of synchronous reluctance motors," in *Proc. ICEM'12*, Marseille, France, Sept. 2012, pp. 994–1000.

[19] G. Yang, R. Tomioka, M. Nakano, and T. H. Chin, "Position and speed sensorless control of brushless DC motor based on an adaptive observer," *IEEJ Trans. Ind. Appl.*, vol. 113, pp. 579–586, May 1993.

[20] L. Harnefors and H.-P. Nee, "A general algorithm for speed and position estimation of AC motors," *IEEE Trans. Ind. Electron.*, vol. 47, no. 1, pp. 77–83, Feb. 2000.

[21] W. T. Villet, M. J. Kamper, P. Landsmann, and R. Kennel, "Evaluation of a simplified high frequency injection position sensorless control method for reluctance synchronous machine drives," in *Proc. IET PEMD 2012*, vol. 1, Bristol, UK, Mar. 2012, pp. 1–6.

[22] P. Guglielmi, M. Pastorelli, and A. Vagati, "Impact of cross-saturation in sensorless control of transverse-laminated synchronous reluctance motors," *IEEE Trans. Ind. Electron.*, vol. 53, no. 2, pp. 429–439, Apr. 2006.

[23] L. Harnefors, "Design and analysis of general rotor-flux-oriented vector control systems," *IEEE Trans. Ind. Electron.*, vol. 48, no. 2, pp. 383–390, Apr. 2001.